ISBN: 978-3-95450-232-5 ISSN: 2673-7000 doi:10.18429/JACoW-NAPAC2022-TUPA38

SUBLINEAR INTENSITY RESPONSE OF CERIUM-DOPED YTTRIUM ALUMINIUM GARNET SCREEN WITH CHARGE*

K. P. Wootton†, A. H. Lumpkin, Argonne National Laboratory, Lemont, IL, USA

Abstract

Swap-out injection to the Advanced Photon Source Upgrade storage ring necessitates the injection of ~17 nC electron bunches at 6 GeV. To aid with machine tune-up and to measure the beam size, diagnostic imaging screens are envisaged at several locations in the beam transport line from the booster synchrotron to the storage ring. As such, it is important to determine whether the response of these screens to charge is linear. In the present work, we examine the effect of sublinear intensity quenching of a Cerium-doped Yttrium-Aluminium-Garnet scintillator screen. A 1.3 megapixel FLIR BlackFly monochrome digital camera was used to image the beam at the scintillator. At 7 GeV beam energy leaving the booster, over the charge densities investigated ($\rho \leq 10\,\mathrm{fC\,\mu m^{-2}}$), an approximately 10% reduction of the imaging intensity due to quenching of the scintillator was observed.

INTRODUCTION

Saturation of scintillator screens has represented a challenge for beam imaging at many facilities – in particular linacs – for example recently at Euro-XFEL [1]. At the Advanced Photon Source (APS), prior work on scintillator linearity included experiments on scintillators using the electron linac [2, 3]. Options of imaging techniques for beam profile monitors in the Booster-To-Storage Ring (BTS) transport line have also been considered [4, 5].

This prompts the question: with high-charge bunches through the BTS transport line for the Advanced Photon Source Upgrade (APS-U), will scintillator linearity with charge be a significant detrimental effect? In the present work, we evaluate the intensity response of a Cerium-doped Yttrium-Aluminium-Garnet (Ce:YAG) scintillator screen as a function of incident electron beam intensity. In particular, we evaluate whether charge linearity will inhibit accurate beam size measurements using the profile monitors.

SCINTILLATOR QUENCHING

Scintillator quenching occurs when the charge density of an incident beam depletes the vacancies in the crystal, and the crystal does not produce light output at a rate proportional to the input charge density [6–8]. We consider limits to quenching of the scintillator along the theory of Birks [9]. This results in approximate upper charge density limts of $16\,\mathrm{fC\,\mu m^{-2}}$ for LYSO scintillators [10], and $20\,\mathrm{fC\,\mu m^{-2}}$ for YAG:Ce scintillators [11]. Quenching is possible in Chromox (Al_2O_3:Cr), however contemporary applications of Chromox scintillators for imaging are typically proton rather than electron beams. Optical Transition Radiation (OTR) has no quenching limit: the limit is probably the damage threshold of the material surface. In practice, if an electron bunch is short (~ tens of fs duration), the practical limit for OTR is probably the presence of Coherent Optical Transition Radiation (COTR), which can potentially exceed the intensity of an OTR signal [12]. Even for bunches of ~ps duration, COTR will occur when there is microbunching, or if there is a narrow current spike.

Quenching of the scintillator reduces the light output of the scintillator at locations on the screen with highest charge density. In effect, this results in fitting the 'tails' of the distribution, and essentially it appears that the image of the beam on a scintillator is larger than the rms electron beam size. A useful comparison of the relative performance of different scintillator materials is in Ref. [13].

METHOD

In the present work, we use a 7 GeV electron beam coming from the booster, imaged using the fluorescent screen BTS:FS3 [14].

Charge Density

We evaluate the electron beam size as a bivariate Gaussian distribution, in order to quantify the areal charge density.

The equation of a bivariate Gaussian distribution in coordinates x_i, with means μ_i, and standard deviations σ_i is given by [15]:

$$p = \frac{1}{2\pi\sigma_1\sigma_2}\left(-\frac{1}{2\sigma_1^2}(x_1-\mu_1)^2 - \frac{1}{2\sigma_2^2}(x_2-\mu_2)^2\right). \quad (1)$$

Hence an electron beam with a profile that is Gaussian in two dimensions with root mean square beam sizes σ_1, σ_2, we can describe the peak electron charge density ρ by:

$$\rho = \frac{q}{2\pi\sigma_1\sigma_2}. \quad (2)$$

RESULTS

Regular Beam

We acquired images of the electron beam using the normal Courant-Snyder lattice parameters using BTS:FS3 at charges up to 4.6 nC. Images of the beam on the BTS:FS3 scintillator as a function of charge are illustrated in Fig. 1.

The electron beam distribution was fitted using a bivariate Gaussian distribution. Beam sizes in both horizontal and vertical planes are plotted in Fig. 2. Peak values of the intensity at each charge level are plotted in Fig. 3.

* Work supported by the U.S. Department of Energy, Office of Science, Office of Basic Energy Sciences, under Contract No. DE-AC02-06CH11357.
† kwootton@anl.gov

ISBN: 978-3-95450-232-5 ISSN: 2673-7000 doi:10.18429/JACoW-NAPAC2022-TUPA38

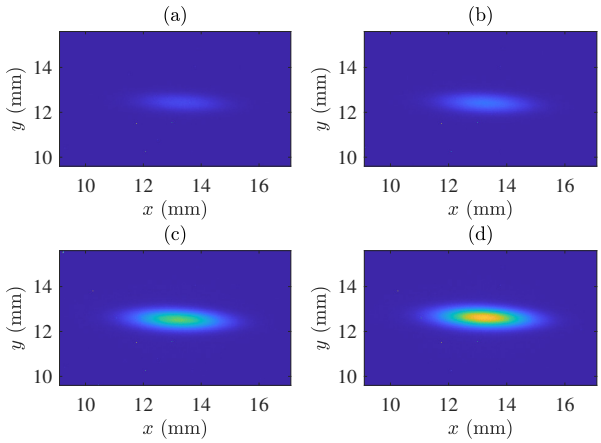

Figure 1: Images of the beam with charge. (a) 0.52 nC. (b) 1.06 nC. (c) 3.2 nC. (d) 4.6 nC.

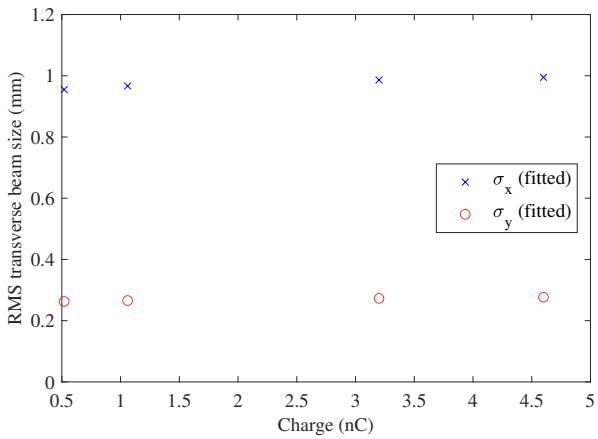

Figure 2: Fitted electron beam sizes as a function of electron beam charge.

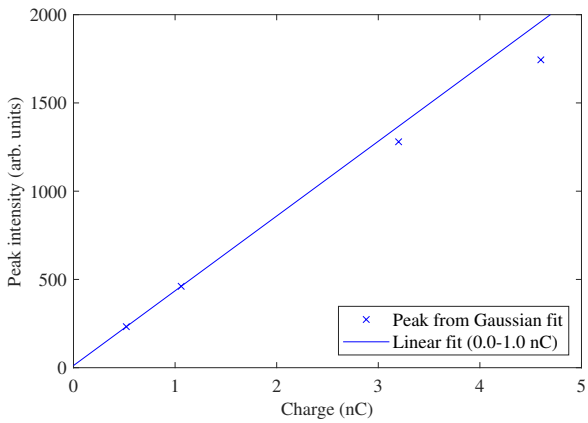

Figure 3: Fitted peak intensity as a function of electron beam charge.

Using Eq. (2), we plot the intensity as a function of the peak charge areal density in Fig. 4.

Focussed Beam

By focussing the electron beam in both planes to form a waist, higher electron beam densities can be achieved for smaller incident bunch charges. The electron beam size was minimised at BTS:FS3 by focussing horizontally and vertically using three upstream quadrupoles (horizontally or vertically focussing). Images of the beam on the BTS:FS3 screen as a function of charge are illustrated in Fig. 5.

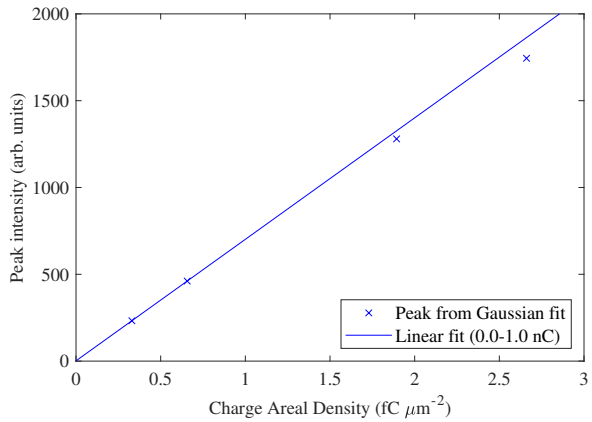

Figure 4: Intensity as a function of peak charge areal density.

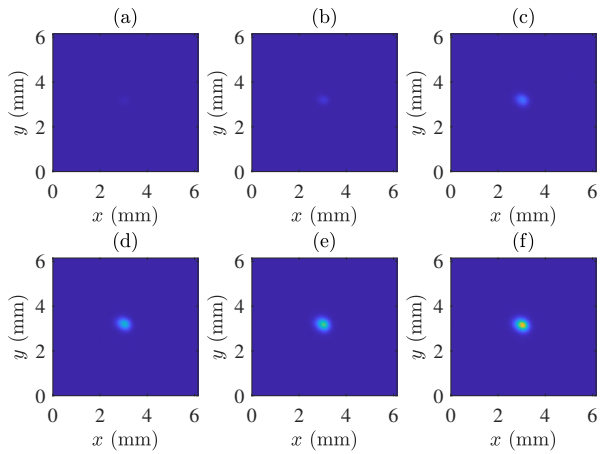

Figure 5: Images of the beam as a function of charge. (a) 0.070 nC. (b) 0.15 nC. (c) 0.50 nC. (d) 1.0 nC. (e) 1.5 nC. (f) 2.0 nC.

The beam distribution was fitted using a bivariate Gaussian distribution. The beam sizes in both planes are plotted in Fig. 6. The peak value of the intensity is plotted as a function of charge in Fig. 7.

Using Eq. (2), the intensity can be plotted against the peak charge areal density, in Fig. 8.

DISCUSSION

Prior work on scintillator responses included analysis of scintillators in the APS linac [2, 3]. The present work was conducted in the BTS, with somewhat larger beam sizes. At the charge densities investigated ($\rho \leq 10\,\mathrm{fC\,\mu m^{-2}}$), even though we start to observe nonlinear behaviour of the scintillator, Figs. 2 and 6 shows negligible change to the measured beam sizes. However, at charge areal densities $\rho \geq 10\,\mathrm{fC\,\mu m^{-2}}$, one should anticipate that the size of

ISBN: 978-3-95450-232-5 ISSN: 2673-7000 doi:10.18429/JACoW-NAPAC2022-TUPA38

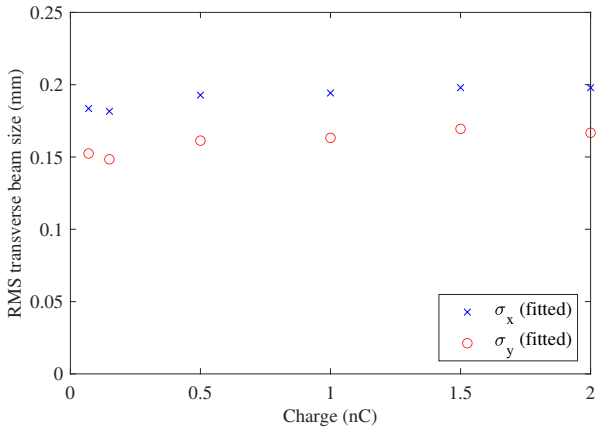

Figure 6: Fitted electron beam sizes as a function of electron beam charge.

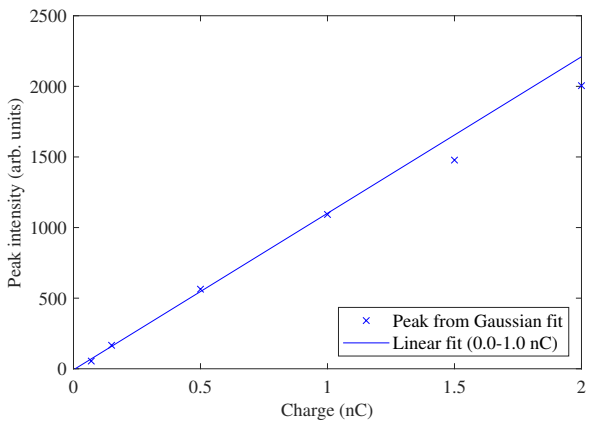

Figure 7: Fitted peak intensity as a function of electron beam charge.

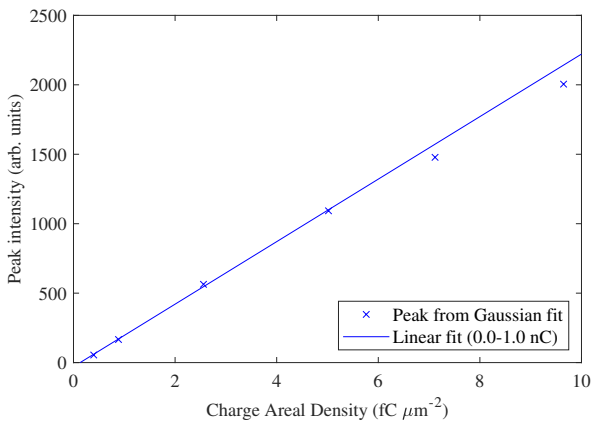

Figure 8: Intensity as a function of peak charge areal density.

the electron beam determined from the scintillation profile would become increasingly unreliable.

SUMMARY

In conclusion, measurements of the electron beam on the BTS:FS3 screen were made. At 7 GeV beam energy leaving the booster, over the charge densities investigated ($\rho \leq 10\,\mathrm{fC}\,\mu\mathrm{m}^{-2}$), an approximately 10% reduction of the imaging intensity due to quenching of the scintillator was observed.

ACKNOWLEDGEMENTS

The submitted manuscript has been created by UChicago Argonne, LLC, Operator of Argonne National Laboratory ("Argonne"). Argonne, a U.S. Department of Energy Office of Science Laboratory, is operated under Contract No. DE-AC02-06CH11357. The U.S. Government retains for itself, and others acting on its behalf, a paid-up nonexclusive, irrevocable worldwide license in said article to reproduce, prepare derivative works, distribute copies to the public, and perform publicly and display publicly, by or on behalf of the Government. The Department of Energy will provide public access to these results of federally sponsored research in accordance with the DOE Public Access Plan. http://energy.gov/downloads/doe-public-access-plan

REFERENCES

[1] G. Kube, S. Liu, A. I. Novokshonov, and M. Scholz, "Identification and Mitigation of Smoke-Ring Effects in Scintillator-Based Electron Beam Images at the European XFEL", in *Proc. FEL'19*, Hamburg, Germany, Aug. 2019, paper WEB01, pp. 301–306. doi:10.18429/JACoW-FEL2019-WEB01

[2] A. H. Lumpkin, B. X. Yang, W. J. Berg, M. White, J. W. Lewellen, S. V. Milton, "Optical techniques for electron-beam characterizations on the APS SASE FEL project", *Nucl. Instrum. Methods Phys. Res. Sect. A*, vol. 429, no. 1, pp. 336-340, 1999. doi:10.1016/S0168-9002(99)00075-3

[3] W. J. Berg, A. Lumpkin, and B. X. Yang, "Characterization of Ce-Doped Scintillating Crystals for Imaging Electron Beams at the APS Linac", in *Proc. LINAC'00*, Monterey, CA, USA, Aug. 2000, paper MOC06, pp. 158–160.

[4] A. H. Lumpkin, private communication, Jan. 2017.

[5] A. H. Lumpkin, W. Berg, J. C. Dooling, K. P. Wootton, and C. Yao, "Proposed Enhanced Imaging Station in the 6-GeV Booster-to-Storage Ring Transport Line for APS Upgrade", in *Proc. NAPAC'19*, Lansing, MI, USA, Sep. 2019, paper TUPLE11, pp. 583–586. doi:10.18429/JACoW-NAPAC2019-TUPLE11

[6] F. Miyahara, S. Kishimoto, M. Satoh, Y. Seimiya, T. Suwada, and M. Koshimizu, "Response of Scintillating Screens to High Charge Density Electron Beam", in *Proc. IPAC'17*, Copenhagen, Denmark, May 2017, paper MOPAB067, pp. 268–270. doi:10.18429/JACoW-IPAC2017-MOPAB067

[7] G. Kube, S. Liu, A. I. Novokshonov, and M. Scholz, "A Simple Model to Describe Smoke Ring Shaped Beam Profile Measurements With Scintillating Screens at the

ISBN: 978-3-95450-232-5 ISSN: 2673-7000 doi:10.18429/JACoW-NAPAC2022-TUPA38

European XFEL", in *Proc. IBIC'18*, Shanghai, China, Sep. 2018, paper WEOC03, pp. 366–370. doi:10.18429/JACoW-IBIC2018-WEOC03

[8] S. A. Payne, W. W. Moses, S. Sheets, L. Ahle, N. J. Cherepy, B. Sturm, S. Dazeley, G. Bizarri, W.-S. Choong, "Nonproportionality of Scintillator Detectors: Theory and Experiment. II", *IEEE Trans. Nucl. Sci.*, vol. 58, no. 6, pp. 3392-3402, Dec. 2011. doi:10.1109/TNS.2011.2167687

[9] J. B. Birks, "Scintillations from Organic Crystals: Specific Fluorescence and Relative Response to Different Radiations", *Proc. Phys. Soc. London*, vol. 64, pp. 874–877, 1951. doi:10.1088/0370-1298/64/10/303

[10] B. Walasek-Höhne, P. Forck, K. Hoehne, R. Ischebeck, and G. Kube, "Screens for High Precision Measurements", in *Proc. IBIC'19*, Malmö, Sweden, Sep. 2019, paper TUBO01, pp. 242–248. doi:10.18429/JACoW-IBIC2019-TUBO01

[11] A. Murokh, J. Rosenzweig, V. Yakimenko, E. Johnson, X. J. Wang, "Limitations On The Resolution Of YAG:Ce Beam Profile Monitor For High Brightness Electron Beam", in *The Physics of High Brightness Beams*, Singapore: World Scientific, pp. 564–580, 2000. doi:10.1142/9789812792181_0038

[12] S. Rimjaem *et al.*, "Comparison of Different Radiators used to Measure the Transverse Characteristics of Low Energy Electron Beams at PITZ", in *Proc. DIPAC'11*, Hamburg, Germany, May 2011, paper TUPD54, pp. 428–430.

[13] R. Ischebeck, E. Prat, V. Thominet, C. Ozkan Loch, "Transverse profile imager for ultrabright electron beams", *Phys. Rev. Spec. Top. Accel. Beams*, vol. 18, no. 8, p. 082802, 2015. doi:10.1103/PhysRevSTAB.18.082802

[14] K. P. Wootton *et al.*, "Horizontal and Vertical Emittance Measurements of the Advanced Photon Source Booster Synchrotron Beam at High Charge", in *Proc. IBIC'19*, Malmö, Sweden, Sep. 2019, pp. 420–424. doi:10.18429/JACoW-IBIC2019-TUPP039

[15] C. B. Do, "The Multivariate Gaussian Distribution", Lecture notes, CS229: Machine Learning, Stanford University, Stanford, CA, USA, Oct. 2008. https://cs229.stanford.edu/section/gaussians.pdf